Q. J. R. Meteorol. Soc. (1998), **124**, pp. 2377–2392

Wind-speed limits in numerically simulated tornadoes with suction vortices

By B. H. FIEDLER*
University of Oklahoma, USA

(Received 11 March 1997; revised 25 November 1997)

SUMMARY

Three-dimensional numerical simulations of tornado-like vortices are presented. Of particular interest is a regime with multiple suction vortices within a larger cyclone. The simulations are designed to assess the magnitude and mechanism by which low pressure is sustained in a suction vortex. The pressure in the transient suction vortices can be nine times that supported by the buoyancy of the 'storm'. The low pressure is sustained by transient axial flow; the pressure-gradient force along the axis is balanced by the inertia of the axial flow, rather than by buoyancy.

KEYWORDS: Numerical simulations Tornadoes Vortex dynamics

1. INTRODUCTION

This paper extends the two-dimensional axisymmetric modelling of Fiedler (1994) and Fiedler (1997) into three-dimensions. The particular subject of interest here is the presence of multiple suction vortices at high swirl ratio in the three-dimensional simulations.

The term *suction vortices* has taken hold in the tornado lexicon primarily as a result of the damage surveys of T. T. Fujita, who surmised that subsidiary vortices with strong low-level inflow were responsible for the accumulation of debris into swaths and spots (Fujita 1971). A review of suction vortices from an observational standpoint can be found by Forbes (1978) and Pauley and Snow (1988). A formal definition of a suction vortex has been offered by Fujita and Forbes (1976); the definition includes a requirement that the vertical acceleration near the surface be greater than the acceleration due to gravity g. Such a definition seems to disallow suction vortices in most laboratory simulations and many numerical models. For example, the models used here do not, and need not, specify g. An alternative definition that emphasizes dynamical processes would require that the perturbation pressure-gradient force along the axis of a suction vortex be mostly balanced by inertia rather than buoyancy. The axisymmetric modelling of Fiedler (1994) shows that when such a balance occurs the axial flow speed will need to be at least as great as the azimuthal flow speed, and there will be strong radial inflow into the base of the suction vortex. The suction vortex will usually be transient and could be terminated above by a vortex breakdown.

The numerical simulations to be presented here are claimed to be relevant to tornadoes despite the fact that there is no simulated thunderstorm and the size of the vortex is greatly enlarged compared with the size of the updraught. The model is able to bring as many grid points to a subsidiary suction vortex within a larger tornado as the model of Grasso and Cotton (1995) brings to the tornado vortex itself. Many of the issues concerning the applicability of these simulations to the atmosphere have been discussed by Fiedler (1994, 1995, 1997). It is claimed that, despite an admittably apparent lack of realism, the simulations are capable of examining how the central pressure deficit in a tornado can be amplified beyond that supported by hydrostatic balance with a buoyancy field.

Here we find that the pressure in the transient suction vortices on the periphery of a larger, parent tornado can be nine times that which could be supported by buoyancy in the 'storm'. Low-level wind speeds in the suction vortices can be 2.5 times greater than those in the hydrostatic, parent vortex. The low pressure is sustained by the inertia of strong,

* Corresponding address: School of Meteorology, University of Oklahoma, 100 East Boyd St. # 1310, Norman, Oklahoma, 73072, USA.

transient, axial flow—consistent with the definition mentioned earlier. Similar amplification was found in axisymmetric suction vortices by Fiedler (1994, 1997). However, strong suction vortices are far more common in these three-dimensional simulations, occurring throughout the high-swirl regime where an axisymmetric simulation would produce only one large, hydrostatic vortex.

2. The model

The numerical experiments are configured similar to those by Fiedler (1994) except that here the computational domain is a box rather than a cylinder. The model has been rendered dimensionless using the depth of the domain and the convective velocity scale. The depth of the domain is 1 and the horizontal widths are 4. The centre of the box is at $(0, 0, \frac{1}{2})$. The bottom boundary is no-slip, the others are free-slip. The fluid has constant density. A fixed buoyancy field for the vertical momentum equation is specified at the centre of the domain:

$$b(x, y, z) = 1.262 \exp\left\{-10x^2 - 10y^2 - 20\left(z - \frac{1}{2}\right)^2\right\} . \tag{1}$$

To allow for seeding secondary instabilities that could break up the vortex, a small, random fluctuation of less than 0.1% of b is added to b. Without this, there would initially only be a wave-number 4 perturbation, due to the box domain, acting on an otherwise axisymmetric vortex. After the formation of the subsidiary vortices, the perturbation in b would have little effect.

The magnitude of b has been chosen to provide the following property. Let the perturbation pressure field divided by the density be denoted as ϕ. In a case where both $\partial\phi/\partial z = 0$ and there are no viscous forces, a parcel accelerating along the central axis of the box would acquire a speed of 1, if accelerating from rest from the lower boundary. On the other hand, in hydrostatic balance, or $\partial\phi/\partial z = b$, the buoyancy is capable of supporting a hydrostatic pressure drop of $\phi|_{z=1} - \phi|_{z=0} = 0.5$ along the central axis. A steady potential vortex around a stagnant core with a pressure drop of 0.5 would have a wind speed of 1. This wind speed of 1 is referred to as the thermodynamic speed limit of the model. (The thermodynamic speed limit is so-named because, in the atmosphere, the wind speed is derived from the convective available potential energy, which is traditionally extracted from a thermodynamic diagram.) Fiedler (1995) discusses the benefits of configuring a model with a thermodynamic speed limit.

A dimensionless viscosity is specified as a function of height:

$$\mu(z) = 1.25 \times 10^{-4} + 2.875 \times 10^{-3} \frac{1 - \cos(\pi z)}{2}. \tag{2}$$

The larger values of μ at the top of the domain control numerical instabilities and limit the effect of energy and vorticity recirculating back into the updraught.

A dimensionless Coriolis parameter f is included to simulate the presence of weak, uniform background rotation. This rotation is assumed to be that of a so-called 'mesocylone' of a thunderstorm, rather than the rotation of the earth. Mesocylones and their generation have been reviewed recently by Rasmussen *et al.* (1994). If this model is to represent thunderstorms, the dimensional depth is of order 10^4 m and the speed limit is of order 100 m s^{-1}, giving a time-scale of 100 s. The dimensionless value of the earth's Coriolis parameter is thus about 0.01. The values of f we use are at least six times this

value: we consider $f = 0.06$, 0.15 and 0.25. Lewellen *et al.* (1997) use much stronger values of background rotation, on the order of 1000 times the earth's rotation.

The model also allows variation of Reynolds number, via the specification of $\mu(z)$ in (2), variation of the geometry of the domain and variation of the distribution of b. An exploration of the sensitivity of the results to Reynolds number might also be especially useful, but the model is rather expensive to run, and could be more so at higher Reynolds numbers, if more grid points were needed. We only vary f in the experiments here.

The grid has $91 \times 91 \times 46$ grid points. The grid is stretched in both the vertical and horizontal (Fig. 1). At the surface, the horizontal grid widths Δx and Δy are less than 0.01 in the region $-0.2 < x < 0.2$ and $-0.2 < y < 0.2$, where the tornado forms. The grid is stretched in the vertical to enhance the resolution in the viscous boundary layer, leaving $\Delta z = 0.0045$ at the lowest level.

The three-dimensional model is basically a fixed-grid version of the model described by Trapp and Fiedler (1995). The model has fifth-order, upwind-biased advection and an iterative solver to maintain a close approximation to incompressibility. A companion two-dimensional, axisymmetric model (Fiedler 1994) is also run in all the experiments. The vertical cross-section shown in Fig. 1 is also the grid for the axisymmetric model.

3. The simulations

The integrations begin at $t = 0$ with no motion. Let U be the wind speed and w be the vertical component of velocity. The maximum of these quantities in the domain as a function of t is shown in Fig. 2. Also shown is the minimum pressure (over density) $\phi_{\min}$, plotted as

$$Q_{\max} \equiv (-2\phi_{\min})^{\frac{1}{2}} . \tag{3}$$

Plotting pressure this way allows it to be conveniently plotted with wind speeds. Also the degree to which the pressure deficit is a dynamic pressure deficit can be assessed by comparing $Q_{\max}$ with $U_{\max}$. Such a comparison strictly requires that $Q_{\max}$ and $U_{\max}$ be sampling the same point, which is usually the case. The fact that $U_{\max}$ is generally less than $Q_{\max}$ shows that either some dissipation has occurred in the flow or that transient effects are substantial. Thus the suction vortex deviates from the idealized dynamics presented by Fiedler and Rotunno (1986).

The first strong spike in all the simulations is a central, axisymmetric vortex, the dynamics of which are discussed by Fiedler (1994, 1997). Of greater interest here is that the three-dimensional simulations for $f = 0.25$ and $f = 0.15$ have suction vortices off the central axis whereas the axisymmetric simulation does not. Of somewhat less interest here is that the three-dimensional and axisymmetric simulations for $f = 0.06$ do not correspond to each other, in either the first spike or the latter spike, despite the fact that the maxima being sampled are central, axisymmetric (or nearly axisymmetric) suction vortices. Except for the difference in the bounds to the domain (box versus cylinder), the simulations could be expected to be the same if the numerical models were both accurate. One possible source of the disparity is the differing amounts of numerical dissipation. For example, in the three-dimensional simulation, numerical dissipation will occur in the azimuthal advection of the azimuthal velocity field; no such dissipation occurs in the axisymmetric simulation.

(a) *The central axisymmetric vortices*

The two-dimensional 'control experiments' will be reviewed first. The nearly steady-state vortices from the axisymmetric model at $t = 55$ are shown in Fig. 3. For $f = 0.15$ and

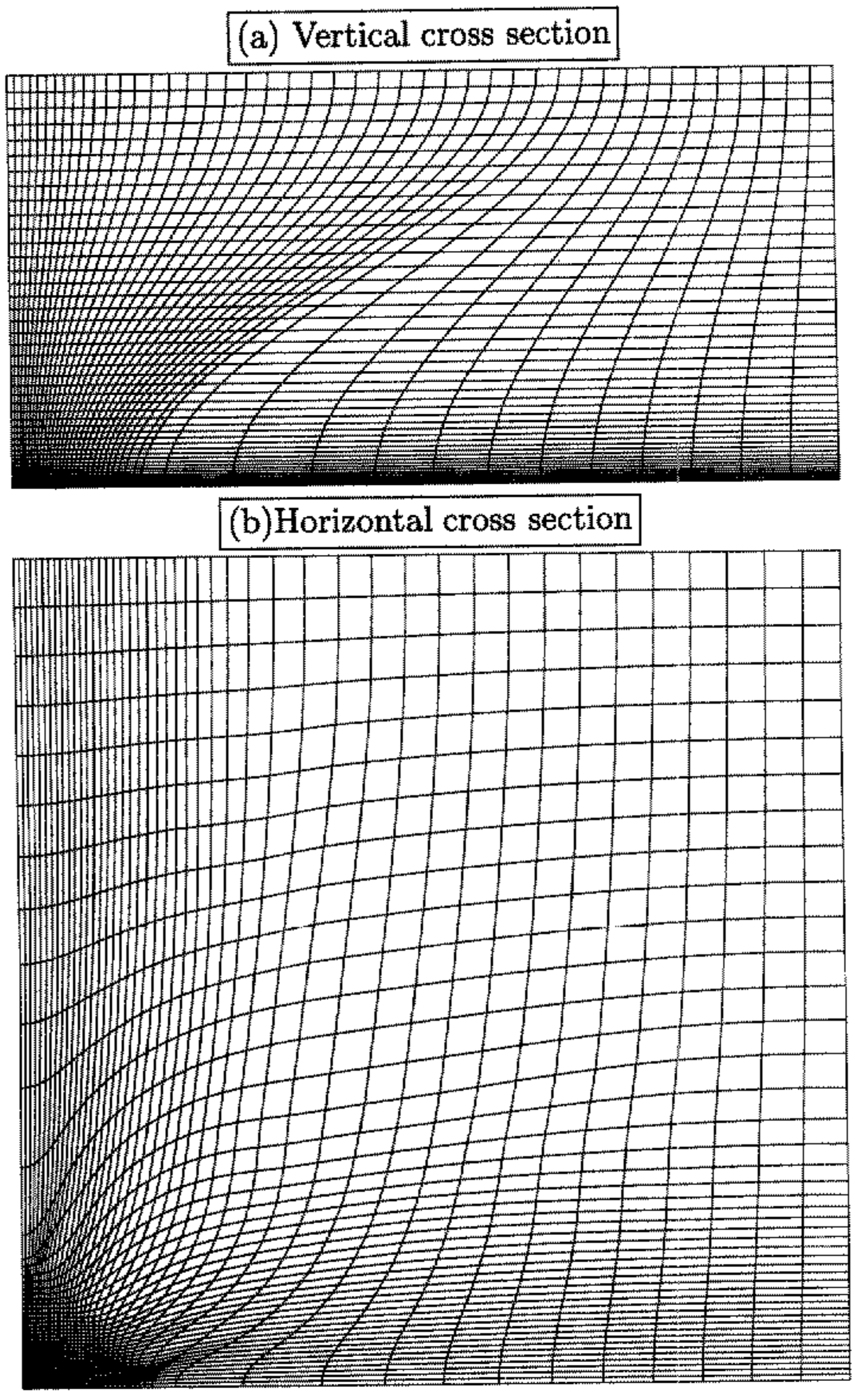

Figure 1. (a) Vertical and (b) horizontal cross-sections of the grid. The vertical cross-section shows $x \geqslant 0$ at $y = 0$. The horizontal cross-section shows the top right quadrant, $x \geqslant 0$ and $y \geqslant 0$ at the surface, $z = 0$.

$f = 0.25$, the core is almost exactly hydrostatic. A larger amount of swirl in the system (i.e. a larger value of f) has not produced a more intense vortex, but a wider vortex.

The three-dimensional simulations all produce a strong axisymmetric vortex initially. With $f = 0.06$, the vortex remains nearly axisymmetric throughout the integration. A close-up of the fields in the second spike for the three-dimensional integration with $f = 0.06$ is shown in Fig. 4. The spike is due to a suction vortex that is centred on the central grid point. Downstream of the vortex breakdown, the vortex has more asymmetry, some of which is evident in Fig. 4 . The presentation of this vortex serves two purposes, though both are a bit subsidiary to the main purpose of this paper. First, an intense vortex

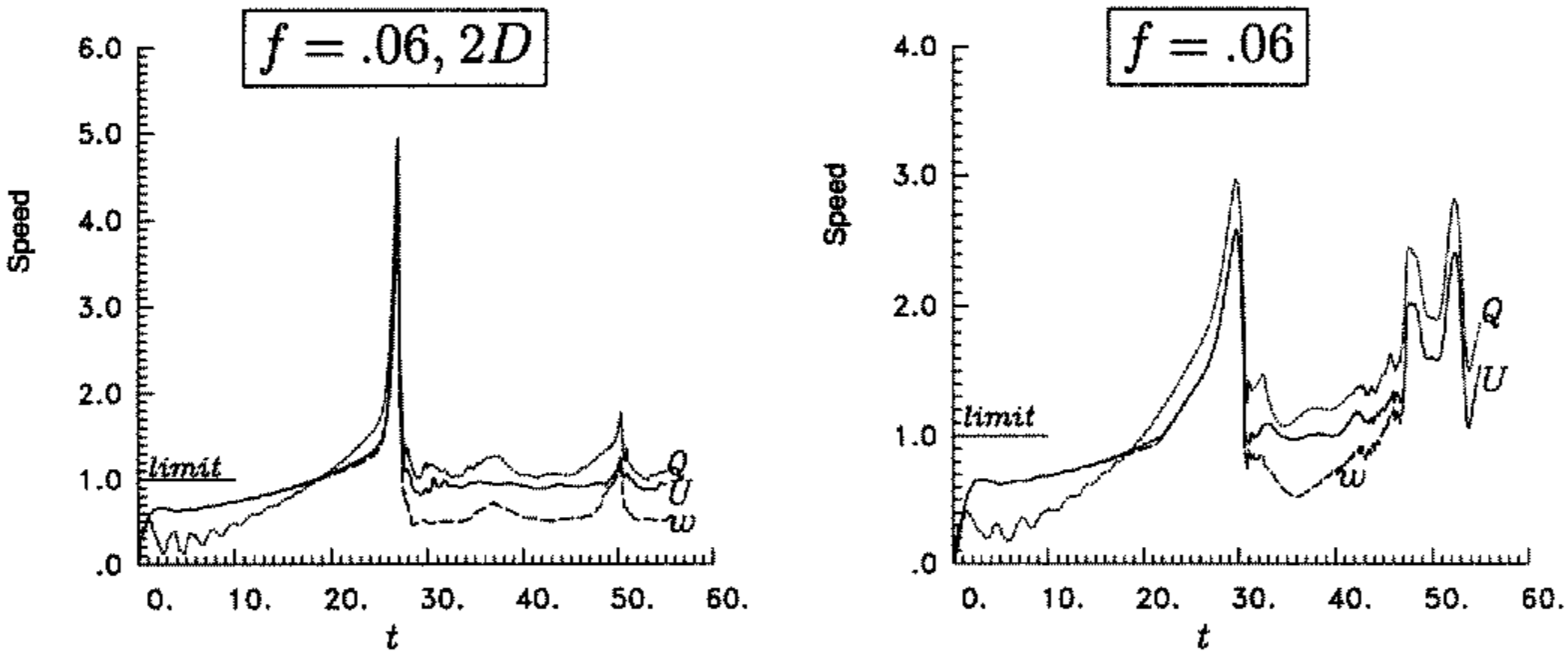

Figure 2. Time histories of the maxima in the domain for, left column, axisymmetric two-dimensional (2D) and, right column, three-dimensional simulations for three values of f, a dimensionless Coriolis parameter, for the wind speed U, for the vertical component of velocity w, and for the minimum pressure Q, see text. One unit of speed is marked *limit*, and is the thermodynamic speed limit of the model.

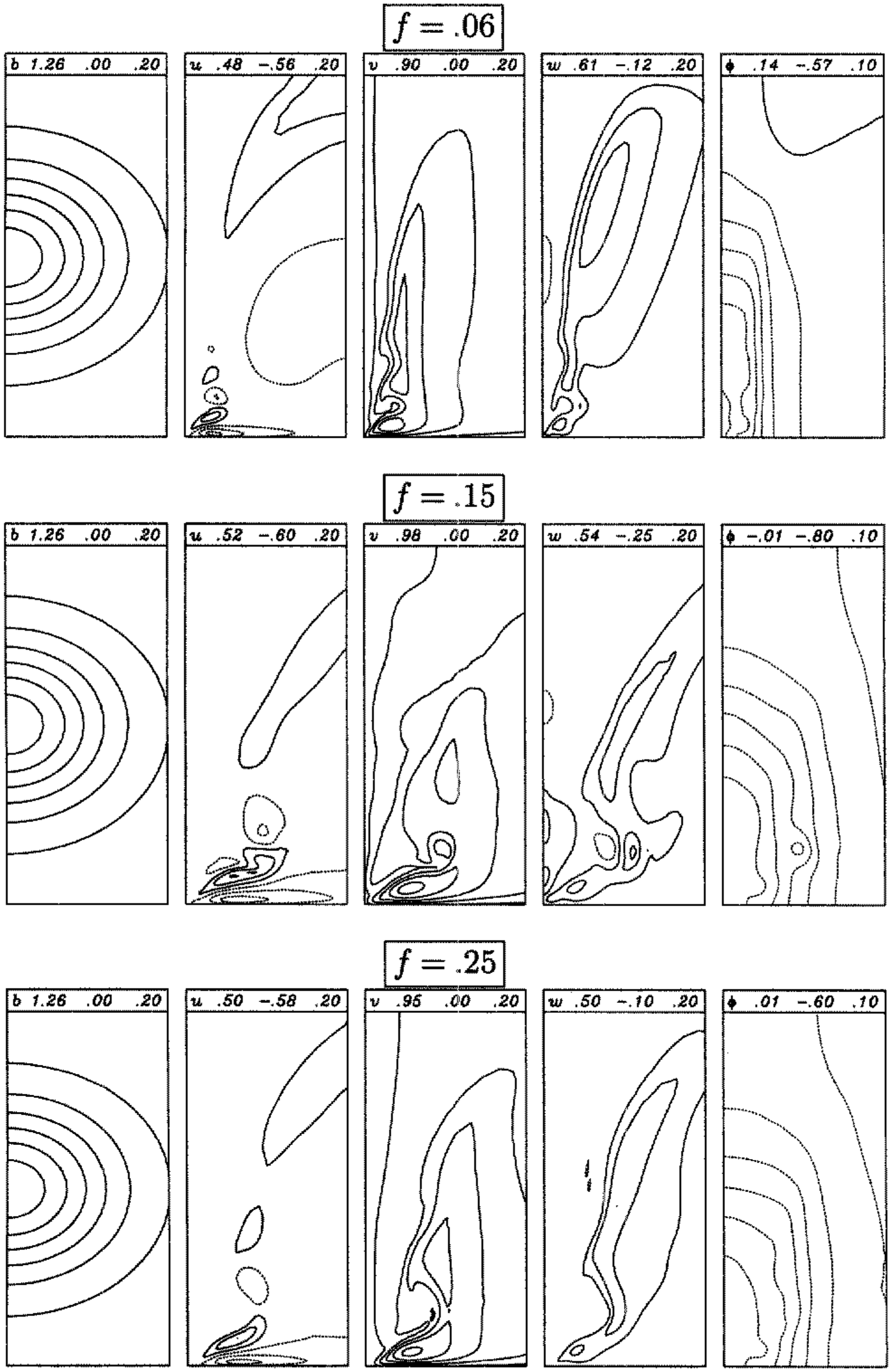

Figure 3. Vertical cross-sections of axisymmetric simulations at $t = 55$ for three values of f, a dimensionless Coriolis parameter. The domain shown is $r < 0.5$, where r is the radial coordinate. In the label, the parameter maximum, minimum and contour interval (see text) are listed, left to right. Positive contours are solid, beginning at one-half the contour interval.

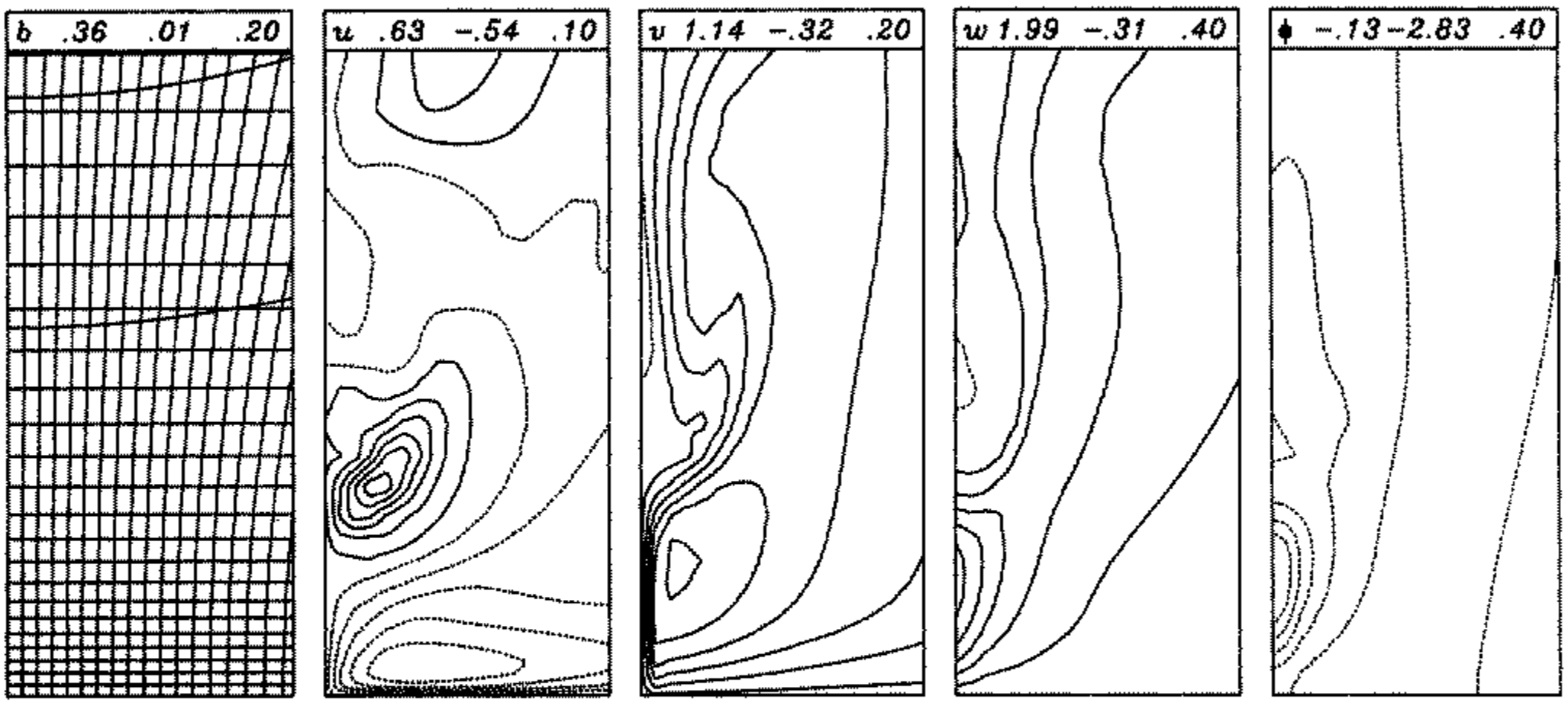

Figure 4. Close-up of the central vortex for the three-dimensional simulation with $f = 0.06$ (see text). The time shown is during the second spike, at $t = 48$. The domain shown is $y = 0$, $0 < x < 0.125$ and $z < 0.25$. The grid is shown superimposed on b at the left. Labels are used as in Fig. 3.

upstream of a vortex breakdown in an axisymmetric model is evidently stable; the dynamics are essentially reproduced with a three-dimensional model. Second, Fig. 4 gives the opportunity to review the dynamics of an axisymmetric suction vortex with a vortex breakdown. Figure 4 shows the strong, low-level axial flow terminated by a vortex breakdown. Immediately below the vortex breakdown, the flow is supercritical in that centrifugal waves cannot propagate downwards from the vortex breakdown. In the core of the strong vortex below the vortex breakdown, the vertical pressure gradient balances the acceleration of the fluid, and is nonhydrostatic. The radial component of the pressure gradient is in nearly cyclostrophic balance.

(*b*) *Multiple suction vortices*

The three-dimensional simulations with $f = 0.15$ and $f = 0.25$ show nearly periodic fluctuations with a period of order 1.5 in the latter part of the integrations. The high amplitudes in these cycles occur in small vortices very near the surface. At times there are two subsidiary vortices on opposite sides of the main vortex, with both being of nearly equal magnitude. The most intense events occur with only one of the subsidiary vortices dominating the flow. A prime example of this is the spike at $t = 46.3$ in the $f = 0.25$ integration. That time has the greatest pressure deficit, with $\phi_{\min} = -4.67$. Some fields within the vortex at this time are shown in Figs. 5–7, which show a series of frames beginning one grid level above the surface and skipping every other level up to the 18th level, where $z = 0.151$. The strong axial flow in the core of the suction vortex does not terminate at a symmetrical vortex breakdown as in Fig. 4, rather it seems to become gradually diffuse, bending outward and wrapping clockwise in the updraught sheath surrounding the vortex. It is not clear if supercritical flow ever occurs in this suction vortex; high winds are apparently sustained without it. In contrast, supercritical flow and a vortex breakdown is necessary to sustain a steady suction vortex (Fiedler 1994).

Of special note is how the suction vortices dominate U at low levels, even where friction has reduced the wind speeds of the parent vortex. Figure 8 shows the grid levels 2 through 10, zoomed in on the intense suction vortex. The horizontal velocity vectors show a very asymmetrical flow field around the vortex. At this time the horizontal velocity of

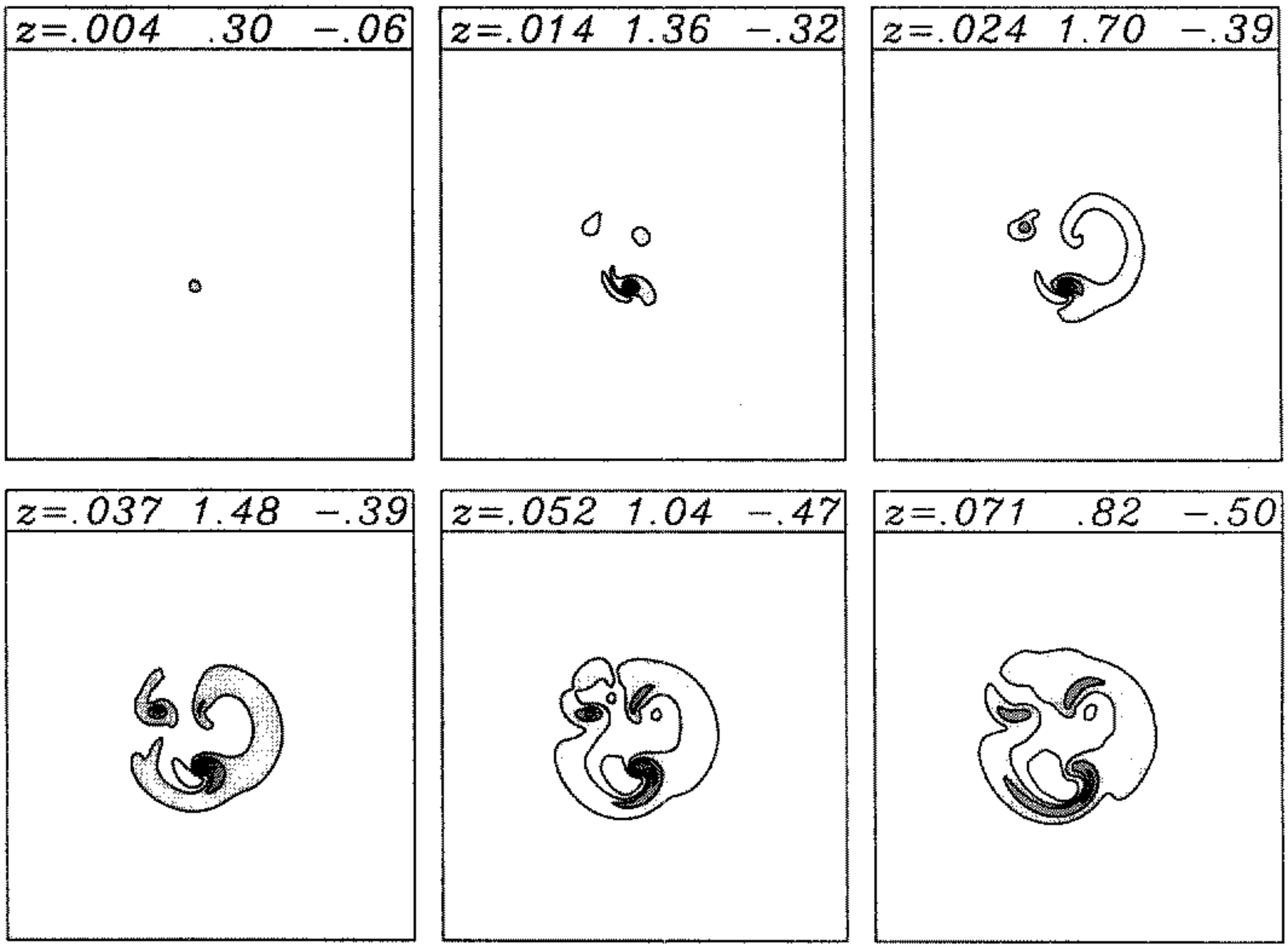

Figure 5. Vertical sequence through a suction vortex showing the vertical velocity w. The labels show the height z and the maximum and minimum of w at $t = 46.3$ and $f = 0.25$ (see text). Shown is $-0.5 < x < 0.5$ and $-0.5 < y < 0.5$. The contour interval is 0.3, beginning at -0.15. White is < -0.15.

translation of the suction vortex is about (0.8, 0). In the frame moving with this translation velocity the flow field is more nearly axisymmetric and reveals how the vortex could be in nearly cyclostrophic balance in that frame (Fig. 9).

A time sequence of the fields through the time of maximum intensity is shown in Fig. 10. The intensification and demise of the suction vortex occurs within 0.8 time units and $\frac{3}{4}$ revolutions of the parent vortex. We can offer here an explanation for the life-time of the suction vortex, in the multiple vortex regime, given its observed maximum vertical extent, but we are not able to offer here a theory for the maximum vertical extent. Although the break-up of a cylindrical vortex sheet into concentrated vorticies may result from a shearing

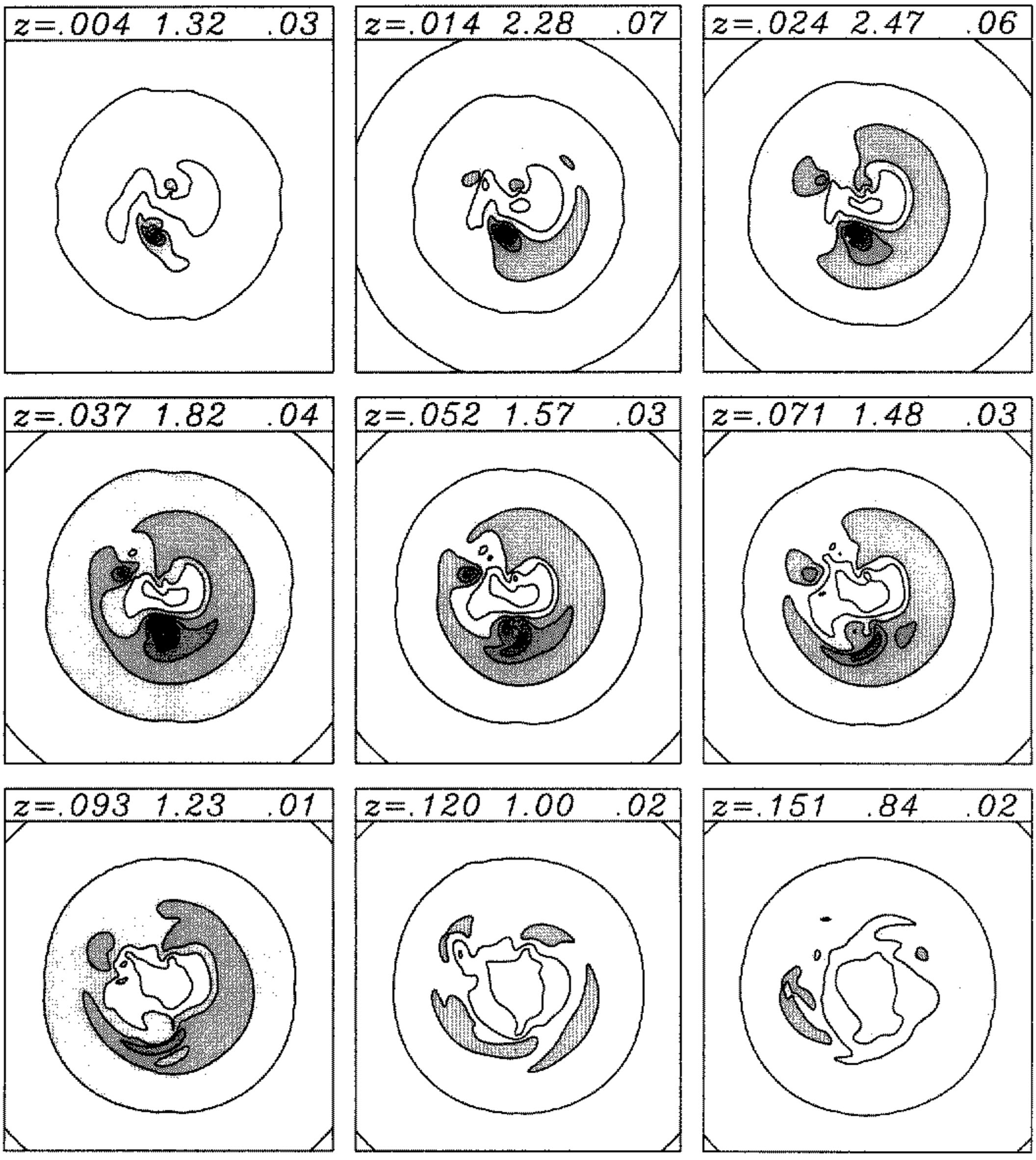

Figure 6. As Fig. 5 but for the total wind speed U. The contour interval is 0.5, beginning at 0.25.

instability, a purely two-dimensional shearing instability cannot provide the amplification of the vorticity, as seen in Fig. 10. Almost certainly this amplification has resulted from stretching along the axis of the vortex. But since the stretching is not uniform, the central pressure and maximum wind speed tend not to develop uniformly along the axis. An axial pressure gradient will develop along the axis. A vortex without a means to sustain an axial pressure gradient, other than by inertia, will tend to equilibrate the pressure along the axis with the propagation of centrifugal waves. Fiedler and Rotunno (1986) review the theory for centrifugal waves of a potential vortex with a non-rotating core. In a reference frame where the axial flow external to the core is zero, the phase speed c for long-wavelength

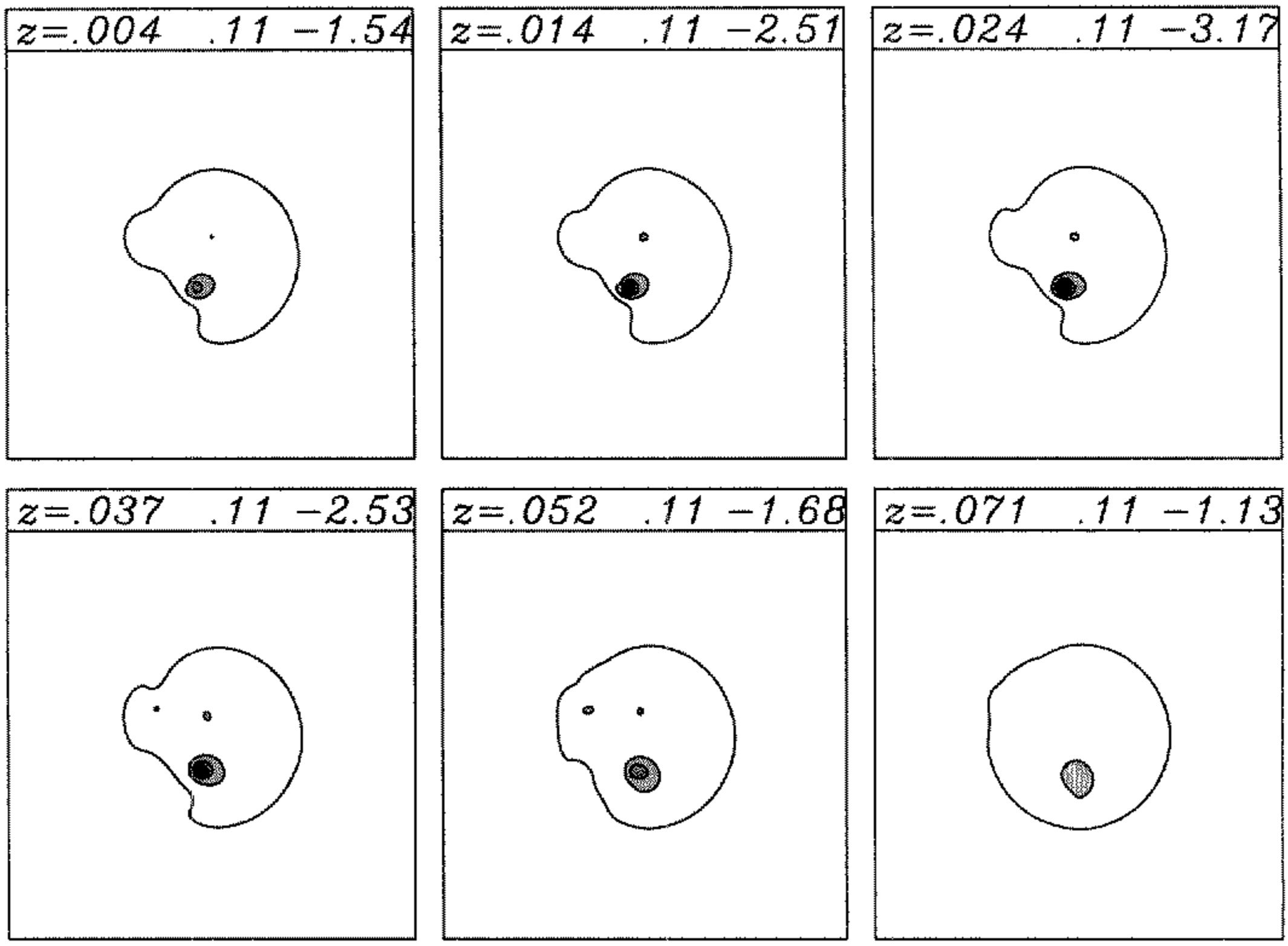

Figure 7. As Fig. 5 but for the pressure ϕ. The contour interval is 0.5, beginning at -0.25.

waves is simply

$$c = w_c \pm \frac{1}{\sqrt{2}} v_c \tag{4}$$

where w_c is the axial velocity in the core of the vortex and v_c is the maximum azimuthal velocity in the potential vortex, at the core wall.

The upper end of the suction vortex will be sampling the pressure of the larger tornado. This pressure will tend to impose itself along the axis at the speed at which centrifugal waves can travel down the axis. Although (4) is from a highly idealized model, we can use (4) to estimate the phase speed of such waves in our simulations. If w_c is not large

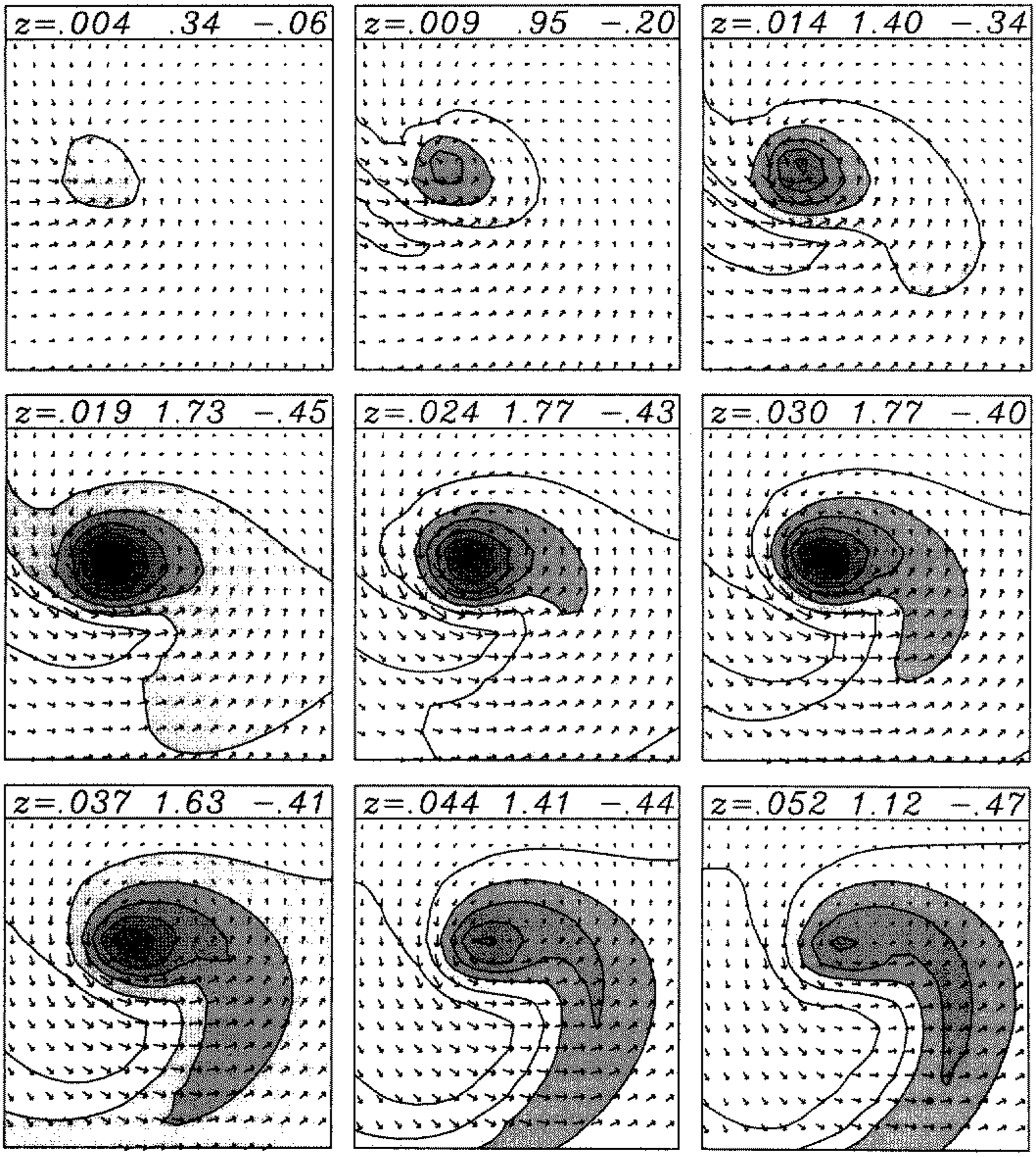

Figure 8. Close-up of the suction vortex for $f = 0.25$ and at $t = 46.3$ at the lowest levels ($z = 0$ excluded). $-0.07 < x < 0.05$, $-0.15 < y < -0.03$. The contours show the vertical component of the wind w with contour interval 0.3 beginning at -0.15. The labels show the height z and the maximum and minimum of w. The vectors show the horizontal velocity (u, v); the maximum magnitude is 2.37 at $z = 0.019$.

enough to render the flow supercritial (meaning not large enough to render all values of c positive) then *the downward phase speed could be a significant fraction of* v_c. Now, with v_c of order the wind speed of that of the parent tornado, and with the observation that in our simulations the suction vortices do not extend higher than approximately the radius of the parent tornado, it is a trivial exercise to estimate that the lifetime of the vortex is of the order of the period of rotation of the parent vortex.

Notice that (4) shows that the magnitude of c increases with v_c. Thus, as a suction vortex intensifies, centrifugal waves should be more effective at equilibrating the pressure along the axis of the suction vortex. In purely two-dimensional studies of vortex dynamics

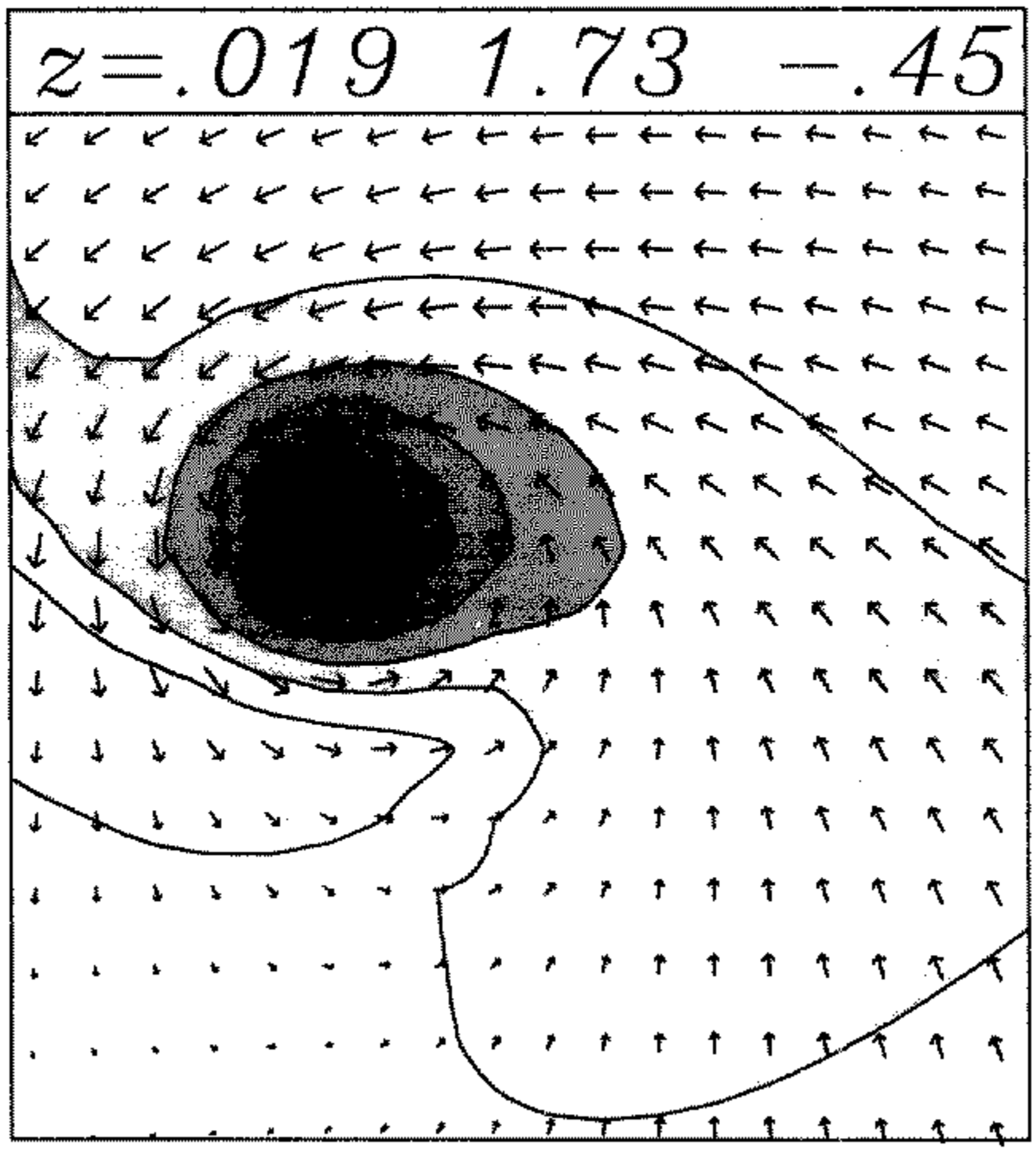

Figure 9. As in Fig. 8 but in a frame moving with the suction vortex at grid level 5 ($z = 0.19$). The label shows the height z and the maximum and minimum of w. The vectors show the horizontal velocity (u, v); the maximum magnitude is 1.95.

and instabilities, the issue of pressure equilibration along the axis of a vortex never arises: a vortex would be uniform along an infinite axis. In suction vortices such as the ones here, we must keep in mind that differential stretching must battle against the equilibration if differential intensity is to be maintained. This is a battle increasingly difficult to win as the vortex intensifies. The suction vortex in Fig. 6 achieved a wind speed of 2.47 before a downdraught broadened its core. We are not able to offer here a complete theory for why this maxima has the value that it does. Nor are we able to offer any empirical rules for what this value would be at the Reynolds number of a real tornado.

4. Conclusions

The results here show that a high swirl vortex can contain subsidiary suction vortices with a maximum wind speed typically ranging from 1.3 to 2.4 times the thermodynamic speed limit. The maximum wind speeds occur very near the lower boundary, within 2% of the depth of the domain. These numbers are in excess of the range from 0.72 to 1.38 that was measured by Bluestein *et al.* (1993) with a portable Doppler radar. (Note that Bluestein *et al.* (1993) include a factor of 0.71 in their definition of the thermodynamic speed limit. The speed limit of 0.71, rather than 1.0, can be used to characterize the maximum wind speed in a hydrostatic Rankine vortex—a simple model for a steady, stable tornado.)

This paper has highlighted a mechanism that could produce peak wind speeds greater than those yet measured (reliably) in the atmosphere. In the simulations, the large wind speeds are happening close to the ground and in a small volume. Furthermore, with the

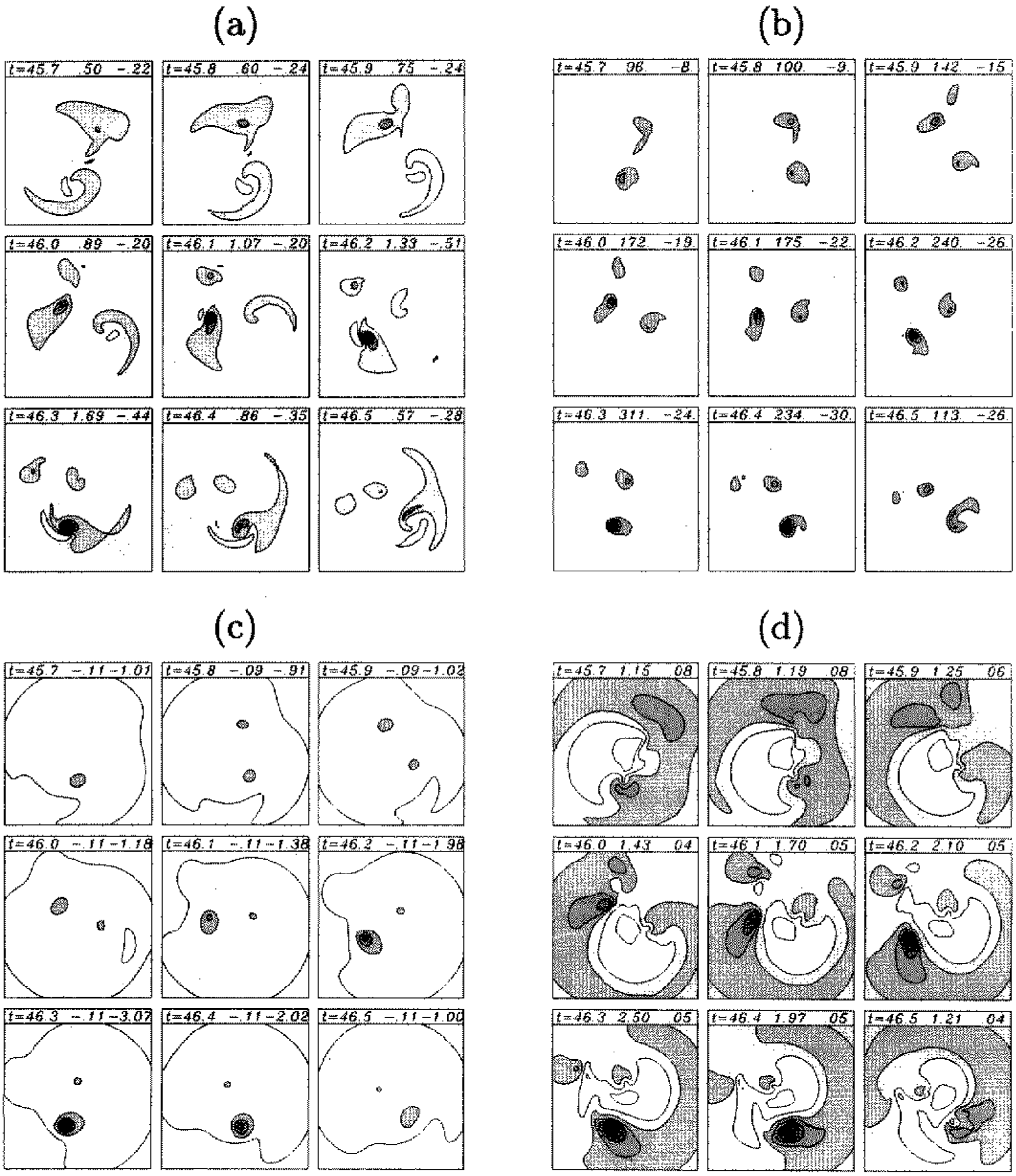

Figure 10. Time sequence showing the intensification of a suction vortex of (a) vertical velocity w, (b) vertical vorticity ζ, (c) pressure ϕ, and (d) total wind speed U for $f = 0.25$ (see text). Shown is $z = 0.019$, $-0.2 < x < 0.2$, and $-0.2 < y < 0.2$. The labels show the time and the maximum and minimum values.

Figure 11. A high-swirl vortex in the Purdue University tornado vortex simulator, visualized with a kerosene fog seeping from around a disk on the bottom of the chamber. A subsidiary vortex is seen on the right of the main vortex.

largest wind speeds being transient, it should not be too surprising if the greatest wind speed in a real tornado is difficult to sample.

Suction vortices like the ones simulated here are certainly good candidates for what Fujita (1971) has described suction vortices to be: explosive in development and often lasting less than one rotation of the parent vortex.

The simulations here are consistent with the laboratory models of tornadoes. Figure 11 in particular looks like a good example of what we have simulated. Snow *et al.* (1980) measure the surface pressure fields in laboratory tornadoes, but state that "the high-frequency fluctuations due to subsidiary vortices were filtered out". They show that the central pressure deficit saturates, or reaches an upper limit, as 'swirl' is increased (swirl meaning the swirl ratio S in their model and f in our model). Except for very large swirl, where the core size becomes a significant fraction of the chamber, and begins to 'choke off' the chamber, the radius of maximum wind increases linearly with swirl, to keep the maximum wind speed constant and independent of S (Baker and Church 1979). These fundamental results can also be seen in Wilkens and Diamond (1987) and Church and Snow (1993). The point of consistency of the laboratory measurements and the numerical simulations is this: most of the tornado for the most of the time is effectively regulated by the natural enforcement of weak axial pressure gradients, except for those in balance with gravity. This principle is easily seen in Church and Snow (1985, 1993) and Pauley (1989). In the laboratory apparatus, the tornado acts as a conduit, or pipe, that samples a pressure deficit at the baffle, downstream towards the fan. Similarly, in the numerical simulations,

the main vortex in a state of maturity acts as a conduit by which the tornado samples the downstream buoyancy. Trapp and Davies-Jones (1997) have explicitly investigated the progression by which the thermodynamic speed limit is enforced along the length of a maturing tornado, in the so-called 'dynamic pipe effect'.

As already shown by Fiedler (1994), special circumstances can escape the enforcement of the thermodynamic speed limit. Here we have shown that the presence of transient suction vortices orbiting within a parent tornado is one more such circumstance. In the simulations we conducted with $f = 0.25$, the mature tornado always contained at least one suction vortex in some stage in development. When a suction vortex achieved its maximum intensity, the wind speed could be greater than 2. This research has not revealed the rules about what controls the magnitude of this peak amplification. The main point here is that the peak amplification is certainly significant and common in the simulated vortices, leading us to believe it could also be significant and common in tornadoes. These results are exactly in line with the deduction of Fujita (1971), who estimated that a suction vortex would have a wind speed twice that of the parent vortex.

Acknowledgement

This work was funded by the National Science Foundation of the USA under grant ATM-9521759.

References

Baker, G. L. and Church, C. R. 1979 Measurements of core radii and peak velocities in modeled atmospheric vortices. *J. Atmos. Sci.*, **36,** 2413–2424

Bluestein, H. B., LaDue, J. G., Stein, H. and Speheger, D. 1993 Doppler radar wind spectra of supercell tornadoes. *Mon. Weather Rev.*, **121,** 2200–2221

Church, C. R. and Snow, J. T. 1985 Measurements of axial pressures in tornado-like vortices. *J. Atmos. Sci.*, **42,** 576–582

1993 'Laboratory models of tornadoes'. Pp. 277–295 in *The tornado: its structure, dynamics, prediction and hazards*. American Geophysical Union monograph series, Vol. 79.

Fiedler, B. H. 1994 The thermodynamic speed limit and its violation in axisymmetric numerical simulations of tornado-like vortices. *Atmos.–Ocean*, **32,** 335–359

1995 On modelling tornadoes in isolation from the parent storm. *Atmos.–Ocean*, **33,** 501–512

1997 Compressibility and windspeed limits in tornadoes. *Atmos.–Ocean*, **35,** 93–107

Fiedler, B. H. and Rotunno, R. 1986 A theory for maximum windspeeds in tornado-like vortices. *J. Atmos. Sci.*, **43,** 2328–2340

Forbes, G. S. 1978 'Three scales of motion associated with tornadoes'. US Nuclear Regulatory Commission, NTIS NUREG/CR-0363

Fujita, T. T. 1971 'Proposed mechanism of suction spots accompanied by tornadoes'. Pp. 208–213 in Preprints of the seventh conference on severe local storms. American Meteorological Society, Boston, USA

Fujita, T. T. and Forbes, G. S. 1976 'Definition of suction vortices.' P. 79 in Proceedings of the symposium on tornadoes. Texas Technical University, Lubbock, USA

Grasso, L. D. and Cotton, W. R. 1995 Numerical simulation of a tornado vortex. *J. Atmos. Sci.*, **52,** 1192–1203

Lewellen, W. S., Lewellen, D. C. and Sykes, R. I. 1997 Large-eddy simulation of a tornado's interaction with the surface. *J. Atmos. Sci.*, **54,** 581–605

Pauley, R. L. 1989 Laboratory measurements of axial pressures in two-celled tornado-like vortices. *J. Atmos. Sci.*, **46,** 3392–3399

Pauley, R. L. and Snow, J. T. 1988 On the kinematics and dynamics of the 18 July Minneapolis tornado. *Mon. Weather Rev.*, **116,** 2732–2736

Rasmussen, E. N., Straka, J. M., Davies-Jones, R., Doswell III, C. A., Carr, F. H., Eilts, M. D. and MacGorman, D. R. 1994 Verifications of the Origins of Rotation in Tornadoes EXperiment: VORTEX. *Bull. Am. Meteorol. Soc.*, **75,** 995–1006

Snow, J. T., Church, C. R. and Barnhart, B. J. 1980 An investigation of the surface pressure fields beneath simulated tornado cyclones. *J. Atmos. Sci.*, **37,** 1013–1026

Trapp, R. J. and Davies-Jones, R. 1997 Tornadogenesis with and without a dynamic pipe effect. *J. Atmos. Sci.*, **54,** 113–133

Trapp, R. J. and Fiedler, B. H. 1995 Tornado-like vortexgenesis in a simplified numerical model. *J. Atmos. Sci.*, **52,** 3757–3778

Wilkins, E. M. and Diamond, C. J. 1987 Effects of convection cell geometry on simulated tornadoes. *J. Atmos. Sci.*, **44,** 140–147